How to cite: *Angew. Chem. Int. Ed.* **2023**, *62*, e202305178
doi.org/10.1002/anie.202305178

Synthetic Biology

Secretion-Catalyzed Assembly of Protein Biomaterials on a Bacterial Membrane Surface

*Qi Xie, Sea On Lee, Nitya Vissamsetti, Sikao Guo, Margaret E. Johnson, and Stephen D. Fried**

Abstract: Protein-based biomaterials have played a key role in tissue engineering, and additional exciting applications as self-healing materials and sustainable polymers are emerging. Over the past few decades, recombinant expression and production of various fibrous proteins from microbes have been demonstrated; however, the resulting proteins typically must then be purified and processed by humans to form usable fibers and materials. Here, we show that the Gram-positive bacterium *Bacillus subtilis* can be programmed to secrete silk through its translocon via an orthogonal signal peptide/peptidase pair. Surprisingly, we discover that this translocation mechanism drives the silk proteins to assemble into fibers spontaneously on the cell surface, in a process we call secretion-catalyzed assembly (SCA). Secreted silk fibers form self-healing hydrogels with minimal processing. Alternatively, the fibers retained on the membrane provide a facile route to create engineered living materials from *Bacillus* cells. This work provides a blueprint to achieve autonomous assembly of protein biomaterials in useful morphologies directly from microbial factories.

Introduction

Protein-based biomaterials have recently attracted attention because of their multifaceted uses in biomedical applications as well as emerging applications as a sustainable material.[1–4] Like other biomaterials, proteins tend to be biocompatible and biodegradable, though they are also genetically-encodable and programmable.[5] Recombinant approaches have been explored to obtain long-chain protein materials that can form fibrous assemblies with superior mechanical properties.[6] Kaplan and co-workers pioneered the expression of spider silk proteins in *Escherichia coli* (*E. coli*) that can replicate the strength and toughness of natural spider silks.[7] More recently, efforts have focused on the secretion of biomaterials. This strategy has several advantages: (i) it alleviates potential toxicity of the aggregation-prone proteins as they do not remain in the cytosol; (ii) it saves metabolic resources by preventing cells from degrading the fibrous protein precursor; (iii) it allows for material to be recovered directly from industrial fermenters without any lysis step; and (iv) it can potentially enable microbial biofactories to perform "living assembly" by actively processing materials during growth. Finally, secreted fibrous proteins play a key role in forming durable cell-cell interfaces, and thereby serve as building blocks of engineered living materials (ELMs).[8,9]

Previous work by Voigt and co-workers demonstrated the use of a type III secretion system (T3SS) in *Salmonella* to secrete silk proteins (Figure 1A).[10] Eukaryotic cells such as *Pichia pastoris* and baby hamster kidney cells have also been engineered to secrete recombinant silk proteins.[11–13] Most recently, Jin et al. engineered a Gram-positive bacterium, *Corynebacterium glutamicum*, to secrete a repetitive silk protein through its SecYEG translocon (Figure 1B).[14] This represents a particularly promising platform for microbial secretion of biomaterials because Gram-positive cells possess translocons on their single plasma membrane, hence conduction through them results in direct excretion into the extracellular milieu. Moreover, SecYEG can secrete proteins at the same time as they are being synthesized (i.e., cotranslationally), hence in the context of Gram-positive bacteria it could facilitate the secretion of protein fibers of very long length.

In Jin et al. and other previous works, the silk protein was collected by acid precipitation followed by ammonium sulfate fractionation, and spun into fibers by extrusion into ethanol (Figure 1C).[14,15] We wondered though if secreted silk could be processed into fibers autonomously by the microbes themselves, which would alleviate the need for further human intervention to produce useful forms of the material.

In the following, we show that the Gram-positive bacterium *Bacillus subtilis* (*B. subtilis*), can also be directed to secrete silk through SecYEG. We show that in this secretion mechanism, silk protomers spend a considerable amount of time residing on the bacterial membrane surface, which facilitates spontaneous assembly and growth into nanofibrils, in a process we call secretion-catalyzed assembly (SCA). These nanofibers can be converted into hydrogels with minimal manipulation. Moreover, when left on the membrane, these fibers can serve a cement-like function that converts *Bacilli* into ELMs with higher mechanical

[*] Q. Xie, Dr. S. On Lee, N. Vissamsetti, Prof. Dr. S. D. Fried
Department of Chemistry, Johns Hopkins University, 21218 Baltimore, MD (USA)
E-mail: sdfried@jhu.edu
Dr. S. Guo, Prof. Dr. M. E. Johnson, Prof. Dr. S. D. Fried
T. C. Jenkins Department of Biophysics, Johns Hopkins University, 21218 Baltimore, MD (USA)

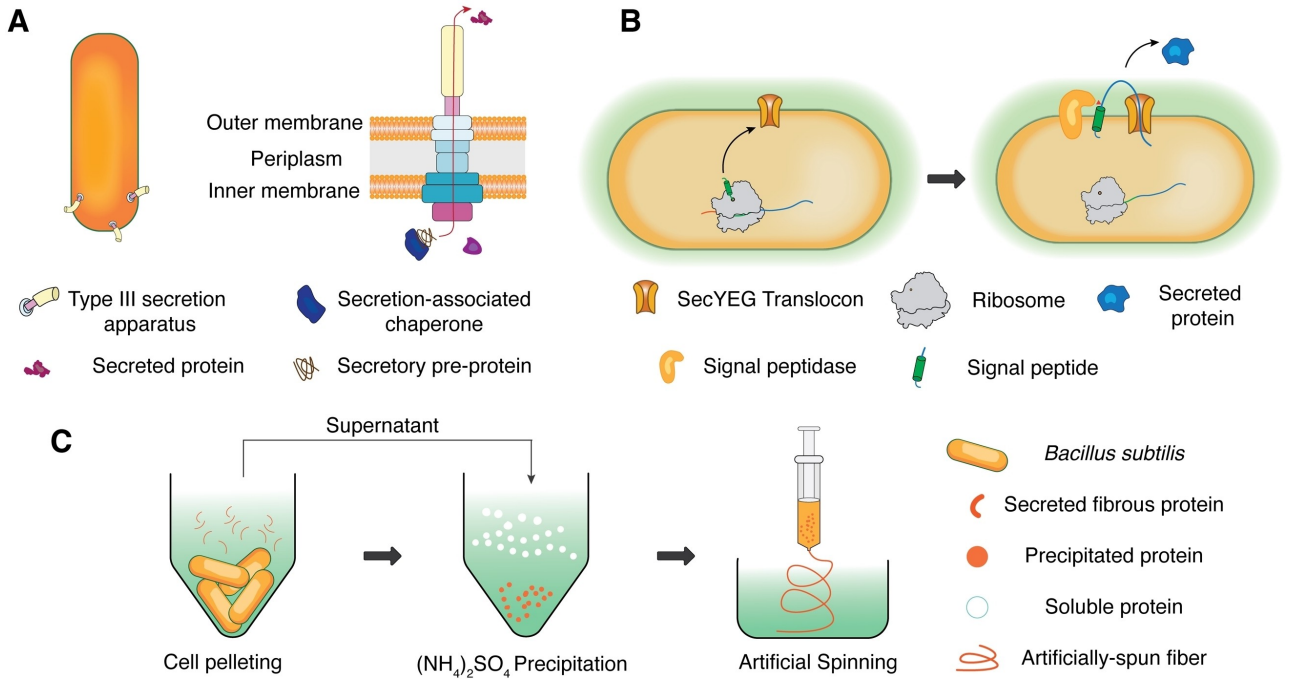

Figure 1. Approaches for the production and purification of protein-based biomaterials from microbial sources. (A) Illustration of the type III secretion apparatus which transports fully-synthesized effector proteins across two membranes. (B) Secretion through the SecYEG translocon in Gram-positive bacteria. The green outline indicates the cell wall while the yellow ellipse indicates the cytosol. (C) Artificial spinning process on purified silk proteins. This has been conducted on secreted silk (purified from growth media),[14] as well as on silk purified from lysates.[15]

stiffness. In summary, our work describes a mechanism for the autonomous assembly of protein biomaterials from microbial factories, and thereby supports SecYEG-translocation in Gram positive bacteria as a promising platform for future protein biomaterial research.

Results and Discussion

Appropriation of the TasA signal for silk secretion

B. subtilis is a popular industrial microbe because of its proficiency at secreting enzymes (e.g., α-amylases, lipases, and proteases), availability of genetic tools, and high level of biosafety.[16,17] Approximately 200 proteins are predicted to be secreted by *B. subtilis* through the SecYEG pathway.[16,18–20] SecYEG translocates proteins in an unfolded state and is responsible for inserting most membrane proteins. In this pathway, the signal sequence is usually looped with the N-terminus facing inward and then further elongation by the ribosome extrudes the nascent protein through (Figure 1B). This generates a pre-protein tethered to the cell via the transmembrane signal peptide. The activity of signal peptidases cleaves off the signal peptide, which liberates the (secreted) mature protein to the extracellular milieu.

To utilize SecYEG for the secretion of heterologous fibrous proteins, we first needed to identify a signal sequence to prepend to the target secretory protein. After a systematic analysis of *Bacillus*'s secretome, we came to the assessment that the TasA signal sequence (TasAss) possessed a unique constellation of features that made it ideal for this purpose (Figure 2A–B, Tables S1–S2, Figure S1).

In the wild, the *tasA* gene encodes the major component of *Bacillus* biofilms (Figure 2B).[21,22] Its signal sequence possesses a clear transmembrane helix (Table S1) and is incompetent for secretion when the factor associated with cotranslational targeting (*ffh*) is deleted (Table S2). These features suggest that the TasA signal sequence is efficiently targeted to the translocon. More importantly, TasAss has a signal peptidase recognition motif that—based on a bioinformatic analysis (Figure S1)—appears to be cleaved by a *dedicated* orthogonal signal peptidase, SipW. We based this assessment on the findings that TasA's signal peptidase recognition site is highly similar to that of TapA, both of which are part of the same operon as *sipW* itself (Figure 2A), but are quite distinct from the standard signal peptidase consensus motif (Figure S1A). Secondly, SipW itself is quite divergent from all the other signal peptidases in *B. subtilis* (Figure S1B–D). These favorable features motivated us to appropriate the TasA signal/cleavage machinery as a module for the general secretion of biomaterials. We cloned the *sipW-tasAss* region (which contains the orthogonal signal peptide-peptidase pair) from the *B. subtilis* genome onto an expression vector (Figure S2). The pLIKE expression plasmid features two stem loops at the 5′ and 3′ termini of the transcribed RNA to promote its stability in the cytosol, the strong *Bacillus* promoter from GroES, and an IPTG (isopropylthio-β-galactoside)-inducible Lac operator.[23–25] This secretion module was installed

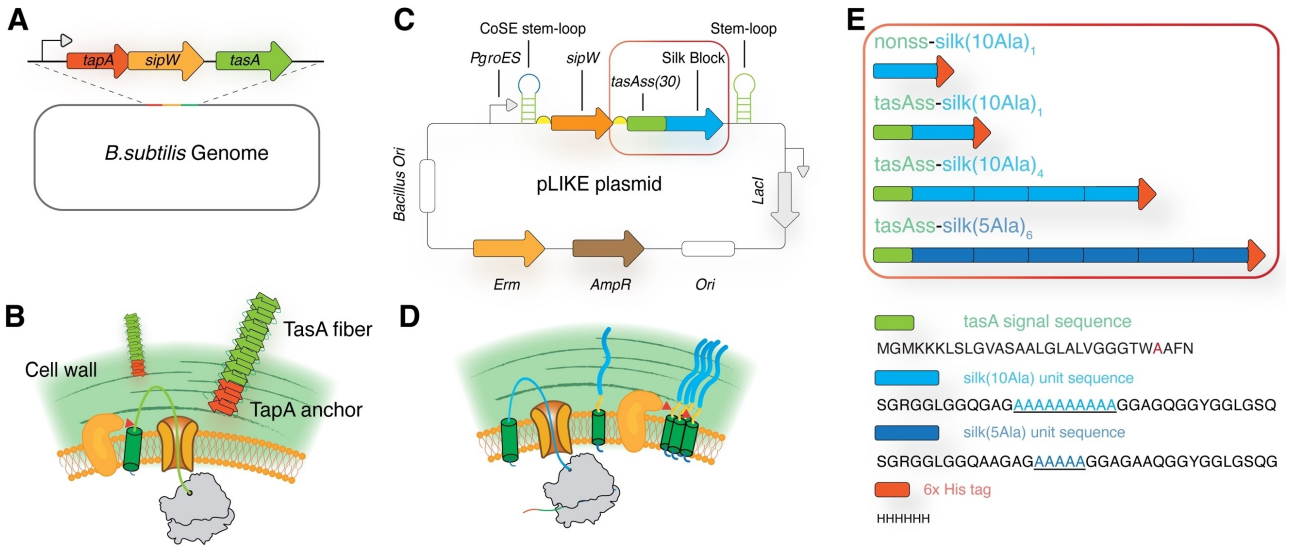

Figure 2. Construction of a TasA secretion system. (A) Illustration of the natural tapA-sipW-tasA operon. (B) Process of natural TasA secretion. The signal peptide is cleaved by SipW (a signal peptidase), and the released TasA forms amyloids seeded by the cell-wall-associated protein, TapA. (C) Map of pLIKE-sipW-tasAss(30)-silk plasmid used to express and secrete silk(10Ala)$_1$ peptide in *B. subtilis*. Amp^R (ampicillin resistance) and Ori allow cloning in *E. coli* while *Bacillus* Ori and Erm (mls resistance) allow expression in *B. subtilis*. LacI enables inducible expression of PgroES. CoSE stem loop incorporates the Lac operator and inhibits mRNA decay. Red box represents where the constructs differ. (D) Illustration of proposed silk secretion and assembly on the membrane. (E) Detailed view of silk variants. Silk sequences with 5 contiguous alanines are denoted silk(5Ala), whilst 10 contiguous alanines are denoted silk(10Ala). The subscript shows the number of repeating silk consensus sequences. Nonss refers to a variant without a signal peptide.

upstream of a single repeat of the consensus silk sequence from major ampullate silk protein 1 (MaSp1) of *Nephila clavipes* with a His-tag (Figure 2C, E); the resulting construct is called pLIKE-tasAss(30)-silk(10Ala)$_1$. Our nomenclature denotes the number of contiguous alanines in the β-crystallite forming region and the number of repeats as a subscript (Figure 2E). We hypothesized that this strategy could enable conduction of the silk protein out of the plasma membrane with subsequent release into the growth medium upon cleavage by SipW (Figure 2D).

Silk is an attractive biomaterial because of its unparalleled mechanical properties (tensile strengths over 1.5 GPa, comparable with steel).[26,27] The molecular basis of silk's strength lies in a repeating module featuring a poly-alanine stretch that can form crystalline beta-sheets with other poly-alanine stretches between chains (effectively acting like crosslinks).[28] The consensus sequence of this module has been widely used in microbial expression;[15,28–31] on the other hand, the propensity of the poly-alanine stretch to aggregate or form beta-hairpins also makes it challenging to secrete.[32]

Detection of secreted silk

We transformed pLIKE-tasAss(30)-silk(10Ala)$_1$ into the mini *Bacillus* PG10—a genome-reduced *B. subtilis* strain that lacks the endogenous *tapA-sipW-tasA* biofilm-forming operon.[33] PG10 has been shown to improve the yield of secreted recombinant proteins due to the deletion of many extracellular proteases.[34,35] Induction of silk(10Ala)$_1$ expression resulted in a negligible growth defect (Figure S3). To test whether the silk(10Ala)$_1$ peptide could be secreted with this system, the secreted fraction was isolated from the supernatant of the centrifuged cell culture. Silk protein in the supernatant was affinity purified with Ni-NTA (nitriloacetic acid) beads and digested with trypsin, and the resulting fragments analyzed with liquid chromatography tandem mass spectrometry (LC–MS/MS). We obtained many MS2 spectra matching peptide sequences associated with silk, with the most frequent sequence corresponding to the expected tryptic fragment of the secreted protein (Figure 3A). The fragmentation pattern in the MS2 spectrum (example shown in Figure 3B) showed clear evidence that the secreted product includes the aggregation-prone poly-alanine stretch. In experiments conducted without trypsinolysis (Figure 3A), we sequenced longer fragments whose N-terminus stretched back to the expected SipW cleavage site on the signal sequence.[21] Because the endogenous *tapA-sipW-tasA* operon is deleted in PG10, these experiments demonstrate that we have successfully reconstituted the TasA secretion apparatus with two components and redirected it to release silk instead of TasA.

We performed western blot analysis on the secreted fraction (S) and the cellular fraction (C, following lysis of the cultured cells), probing for the His-tag on the silk protomer (Figure 3C). In the cellular fraction we detected the expected band below 15 kDa, as the molecular weight (MW) of the silk unit following signal peptidase cleavage would be 5.1 kDa. On the other hand, in the secreted fraction we observed a ladder of MWs separated by roughly 5 or 10 kDa up to 120 kDa, and also entities of very high MW that could not migrate out of the stacking layer of the

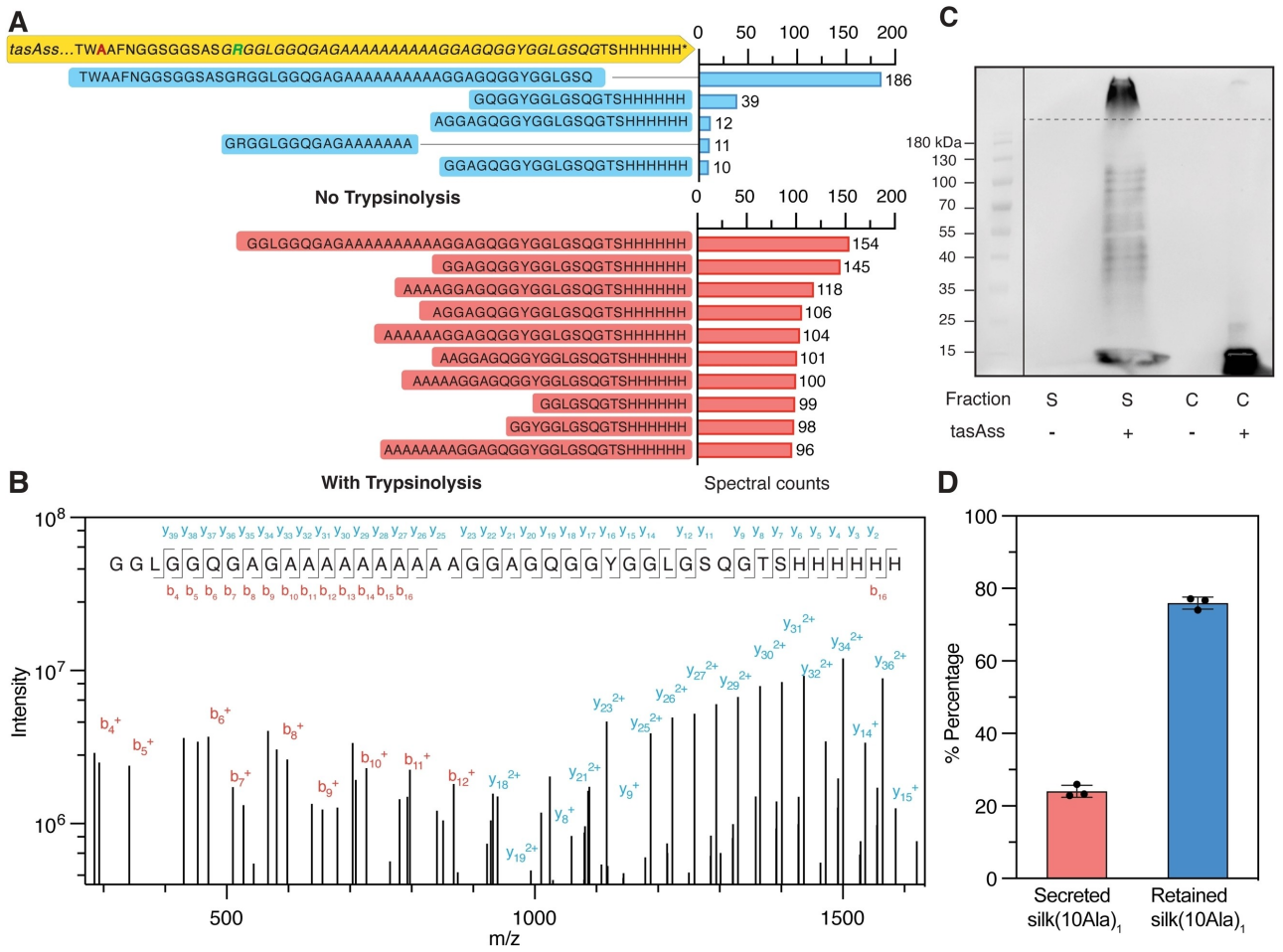

Figure 3. Secretion and assembly of silk(10Ala)$_1$ peptides. (A) Sequenced peptides from the material affinity-purified out of spent media and analyzed by liquid chromatography tandem mass spectrometry (LC–MS/MS), either without (blue) or with (red) trypsinolysis. Bar charts indicate the number of MS2 spectra obtained matching to the given sequence. (B) A sample MS2 fragmentation spectrum corresponding to the most frequently sequenced peptide from secreted material treated with trypsin. (C) Western blot using an anti-His antibody (specific for His-tagged silk(10Ala)$_1$) of samples collected either from the secreted fraction (S) or lysed cells (C, cellular fraction). *B. subtilis* PG10 cells were transformed with pLIKE plasmids that either contained the tasAss upstream of silk(10Ala)$_1$ or not. Dash line indicates the boundary between the stacking layer and resolving layer. Solid line is boundary between two imaging modes, stain-free and chemiluminescence (to acquire the ladder and sample bands respectively; raw images of both are provided as Figures S15–16). Image is representative of three performances of the experiment ($n=3$). (D) The percentage of silk(10Ala)$_1$ that gets secreted or retained based on densitometry of western blots.

gel. These higher aggregates were stable and remained intact even after boiling the samples in sodium dodecyl sulfate (SDS) buffer. Without the signal sequence, no silk was recovered, likely because the short silk(10Ala)$_1$ peptides were degraded in the cytosol before they could assemble (Figure 3C).

Silk proteins form intermolecular crystalline beta-sheets that can be processed into stable nanofibers with high molecular weight.

Nevertheless, we were surprised by the formation of stable high-MW assemblies, as silk fibrilization typically requires downstream processing, such as applying shear forces (such as in spider spinnerets),[36] changing the buffer conditions (e.g., high potassium phosphate),[37,38] or lowering the pH.[13,27,39,40] Moreover, recombinant and natural silk proteins that efficiently fibrillize are typically very long chains (>1,000 residues) consisting of many tandem repeats of the silk unit. Formation of fibrils from silk proteins as small as silk(10Ala)$_1$—30 aa—has not been previously documented, to the best of our knowledge. Indeed, if it is not secreted, silk(10Ala)$_1$ is so unstructured that it is easily proteolyzed (Figure 3C).[41] These observations led us to hypothesize that some aspect of the secretion process was facilitating silk assembly.

Silk assembly occurs on the membrane surface

To interrogate where and when silk protomers assemble into high-MW entities, we employed a biochemical approach (Figure S4) in which four distinct compartments from *Bacillus* were isolated: the cytosol, the cell membrane, the cell wall, and the external media. Western blot analysis on these four fractions at several time points during expression/

secretion confirmed that in the cytosol (Figure S4A), assembly is primarily limited to tetramers ($4\times$silk(10Ala)$_1$). A similar pattern is found on the dense cell wall of *Bacillus* (Figure S4C). On the other hand, on the membrane-associated fraction, we find clear evidence for higher-order assemblies with discrete molecular weight (upto 120 kDa), and then after 8 h the formation of assemblies so large to be unable to migrate during SDS-PAGE (Figure S4B). Only at later times are these silk assemblies fully secreted into the extracellular milieu, where they retain a similar MW profile as observed on the membrane (Figure S4D). These observations lead to the model that silk(10Ala)$_1$ is first translocated through the plasma membrane, where it assembles on the membrane surface, and *then* gets released into the extracellular milieu. The presence of silk retained in the cytosol (Figures 3D, S4A) suggests that secretion is likely occurring in both the cotranslational and post-translational modes.

We reasoned that two features about membrane localization could catalyze assembly. Firstly, peptides confined to move in two dimensions would pay a smaller entropy cost to assemble compared to movement in three dimensions. Indeed, the utility of dimension reduction in biomolecular assembly has been previously demonstrated in several well-known cases (e.g., clathrin-mediated endocytosis and the Z-ring division machinery[42–44]). To see if dimension reduction could facilitate silk assembly as well, we developed a reaction-diffusion model (Figure 4A, see also Supporting Information Methods) in which silk monomers were represented as rigid bodies with four interaction sites, similar to as described previously.[45] The simulations revealed that for a wide range of potential microscopic binding constants (K_D), assembly in 2D (such as on a membrane) could occur rapidly (Figures 4B, S12, Movies S1–S4). The proportion of monomers that remain unassembled at long times was sensitive to K_D, and a K_D of 1 μm appears to match the

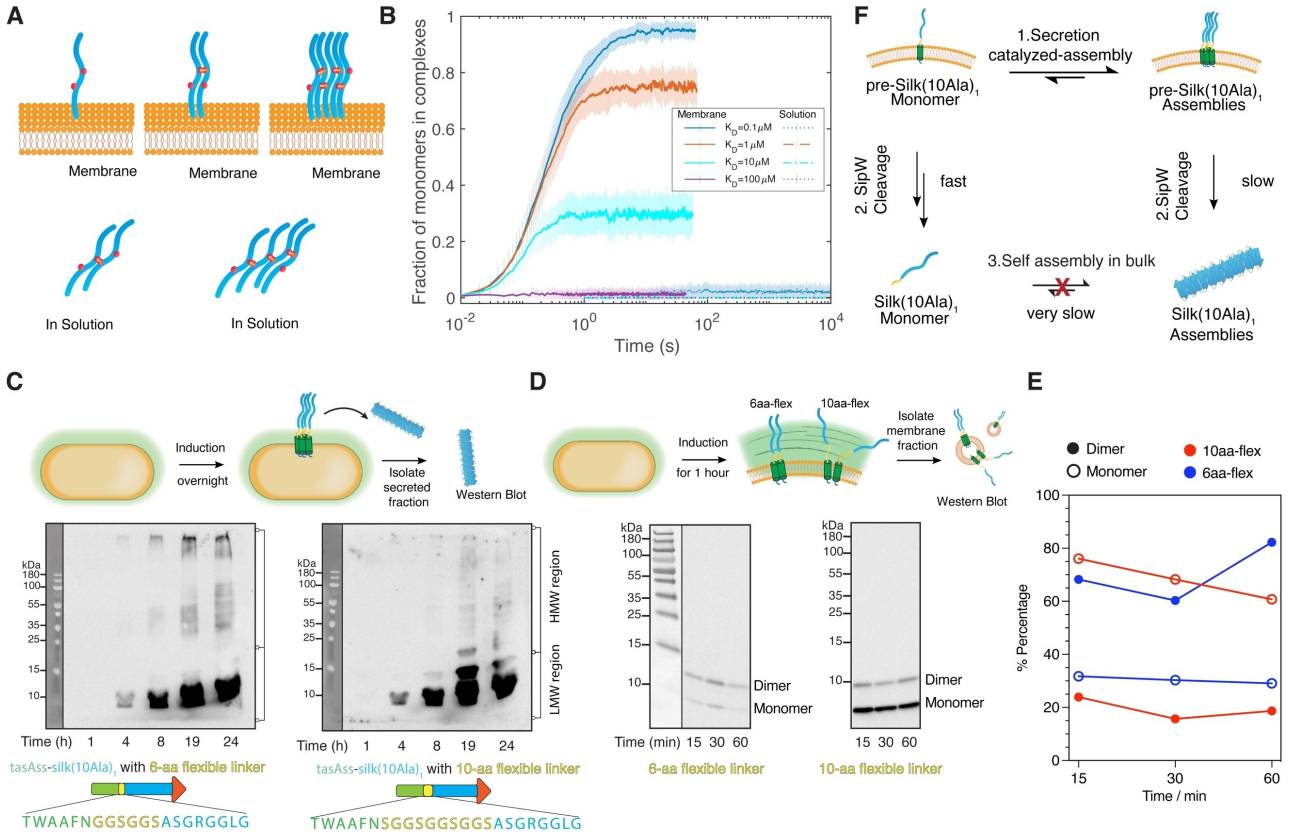

Figure 4. Membrane localization and conformational restriction promote silk assembly. (A) Representation of a silk(10Ala)$_1$ monomer used in reaction-diffusion (RD) simulations.[63] Monomers are assigned a rod shape (blue) with 2 identical binding sites (red, see Supporting Information for details on model construction). Interaction between two sites is represented by yellow lines. One side of the rod contains a binding site to the membrane, which can localize it to the membrane. (B) Time dependence of the fraction of monomers in complexes that contain 5 or more monomers in RD simulations. Error bars represent std dev from replicates ($n=48$). (C) Western blot of secreted fractions from PG10 cells harboring a pLIKE vector in which silk(10Ala)$_1$ (blue) was separated from the signal peptide (green) with either a 6-residue flexible linker or a 10-residue flexible linker (yellow; annotated sequences shown below). Lanes corresponds to samples collected at different time points after induction. (D) Pulse-induction experiment. PG10 cells harboring pLIKE were allowed to express the two linker variants of tasAss-silk(10Ala)$_1$ for 1 hour. The inductions were then paused. Membrane fractions were isolated and processed for western blotting. (C, D) Solid line is boundary between two imaging modes, stain-free and chemiluminescence (to acquire the ladder and sample bands respectively; raw images of both are provided as Figures S17–21). (E) Densitometry of the western blot images from panel D, with intensities plotted as percentages $(\text{x-mer})_t/((\text{monomer})_{15\text{min}} + (\text{dimer})_{15\text{min}}) \times 100\,\%$. (F) Kinetic model of secretion catalyzed assembly of silk(10Ala)$_1$.

experimental data the closest (for which $75\pm5\,\%$ is assembled (Figure 3C)). On the other hand, the simulations show that assembly in 3D (in solution) is not possible for the single-repeat silk monomer at any K_D tested (see also Movies S5–S8).

A second feature we considered is that when silk peptides are tethered to the membrane with a short linker, their conformational freedom would be restricted so that assembly would also involve paying a smaller configurational entropy cost. To test if conformational flexibility also affects assembly, we performed another series of western blots, but this time altered the length of the flexible linker between the membrane-spanning signal peptide and the silk unit (Figure 4C–E). We found that the increased flexibility associated with a 10-aa linker resulted in smaller oligomers and a reduction of the high-MW entities in the secreted fraction (Figure 4C). Hence, we conclude that maintaining silk$(10Ala)_1$ on the membrane with minimal flexibility helps build larger assemblies. To test if conformational flexibility also affected initial assembly events on the membrane, we analyzed the oligomeric state of the two linker-length variants in the membrane fraction following a short 1-h induction, after which only monomer and dimer bands are apparent (Figure 4D). The shorter (6-aa) linker resulted in a high percent of dimer, whereas the 10-aa linker resulted in less silk$(10Ala)_1$ dimer (Figure 4D–E)—supporting the view that the longer linker inhibits assembly.

These experiments suggest that the intermediate stage wherein silk peptides are tethered to the membrane represent a critical period for assembly to occur. To test this, we examined the MW profile of material produced by cultures aged overnight (Figure S5A). Aging resulted in a small increase of high-MW entities and decrease in low-MW species (Figure S5B–C), consistent with the theory that assembly occurs primarily on the membrane, and to a lesser degree in bulk solution following release by signal peptidase.

Integrating these results, we propose the following model for how secretion-catalyzed assembly works (Figure 4F). Pre-silk$(10Ala)_1$ peptides tethered by the TasAss diffuse in the plane of the membrane and—facilitated by a less flexible linker—initially nucleate into a cluster on the membrane surface and form a patch that is resistant to SipW cleavage. On the other hand, isolated silk peptides can be more rapidly released from the membrane. These released peptides kinetically partition into the bulk medium as a monomer, and then remain mostly incompetent at assembling (supported by culture aging (Figure S5)). Initial assembly occurs when silk$(10Ala)_1$ is membrane-tethered through the signal sequence (Figure 4), and then these assemblies are more slowly released by SipW.

Visualization of silk fiber assembly on the membrane

To test the model in Figure 4F more directly and to understand the physical nature of the high-MW bands detected on western blots, we imaged silk$(10Ala)_1$ nanostructures both in vitro and *in cellulo* with electron microscopy (Figure 5). Scanning electron micrographs of purified material recovered from the growth media revealed the formation of fibrous morphologies (Figure 5A–B). Together with transmission electron micrographs we estimate that fibers have typical diameters of $\approx$100 nm (Figure S6). These images are strikingly reminiscent of micrographs of real silk proteins, even though they are derived from polypeptides $\approx10^2$ times longer than the 30-residue silk$(10Ala)_1$.[46–48] We further verified using circular dichroism that these materials consist of beta secondary structure (Figure S7).

Next, we sought to visualize the assembly process on the bacterial membrane. To perform these experiments, we harvested induced *B. subtilis* cells and crosslinked them with glutaraldehyde. The cells were immunostained with Ni-NTA decorated gold nanoparticles, blotted, and imaged with a transmission electron microscope (Figure 5D–I). As we zoomed in, it became clear that these *B. subtilis* cells were indeed autonomously processing silk proteins into fibers on their membrane surface. Moreover, these fibers were specific to *Bacillus* harboring the genetic construct as untransformed cells lacked them (Figure 5D) as did cells harboring a silk-encoding construct lacking the TasA secretion signal (Figure 5G). The specific association of the high-contrast gold nanoparticles to the projections (Figure 5E–F) demonstrates that these objects are composed of silk$(10Ala)_1$, because it alone bears a His-tag.

Generalization to longer silk concatemers

Motivated by these results, we wondered whether secretion catalyzed assembly would also occur for longer silk proteins with more repeats and cloned several variants (see Figure 2E and Supporting Information Methods). Silk$(10Ala)_4$ consists of three additional repeats of the original silk sequence used in our earlier studies. We found however that this construct, when induced, caused cells to grow very slowly (Figure 6). This negative result suggested that the 10-Ala block might be less compatible with secretion, possibly due to its propensity to form beta-sheets before conduction through SecYEG which in turn "clog" the channel. This is anecdotally consistent with a separate study in which silk concatemers that were successfully secreted contained shorter contiguous polyalanine blocks.[14] Hence, we cloned a silk$(5Ala)_6$ variant (cf. Figure 2E), and found that inducing its expression did not result in a large growth defect (Figure 6). Significantly, silk$(5Ala)_6$ also undergoes SCA, and when directly visualized by transmission electron microscopy (Figure 5H–I) generates even more complex and elaborate projections emanating from the cell surface. Significantly, previous work by Jin et al.[14] successfully secreted silk$(5Ala)_{16}$ and silk$(5Ala)_{64}$ from another Gram-positive bacterium through the same translocon (SecYEG) suggesting that silk$(5Ala)_N$ variants are generally secretable via this modality. Hence, it seems promising that SCA could be applied to longer silk concatemers were these variants to be incorporated into the orthogonal signal peptide/signal peptidase system reported here in *Bacillus.*

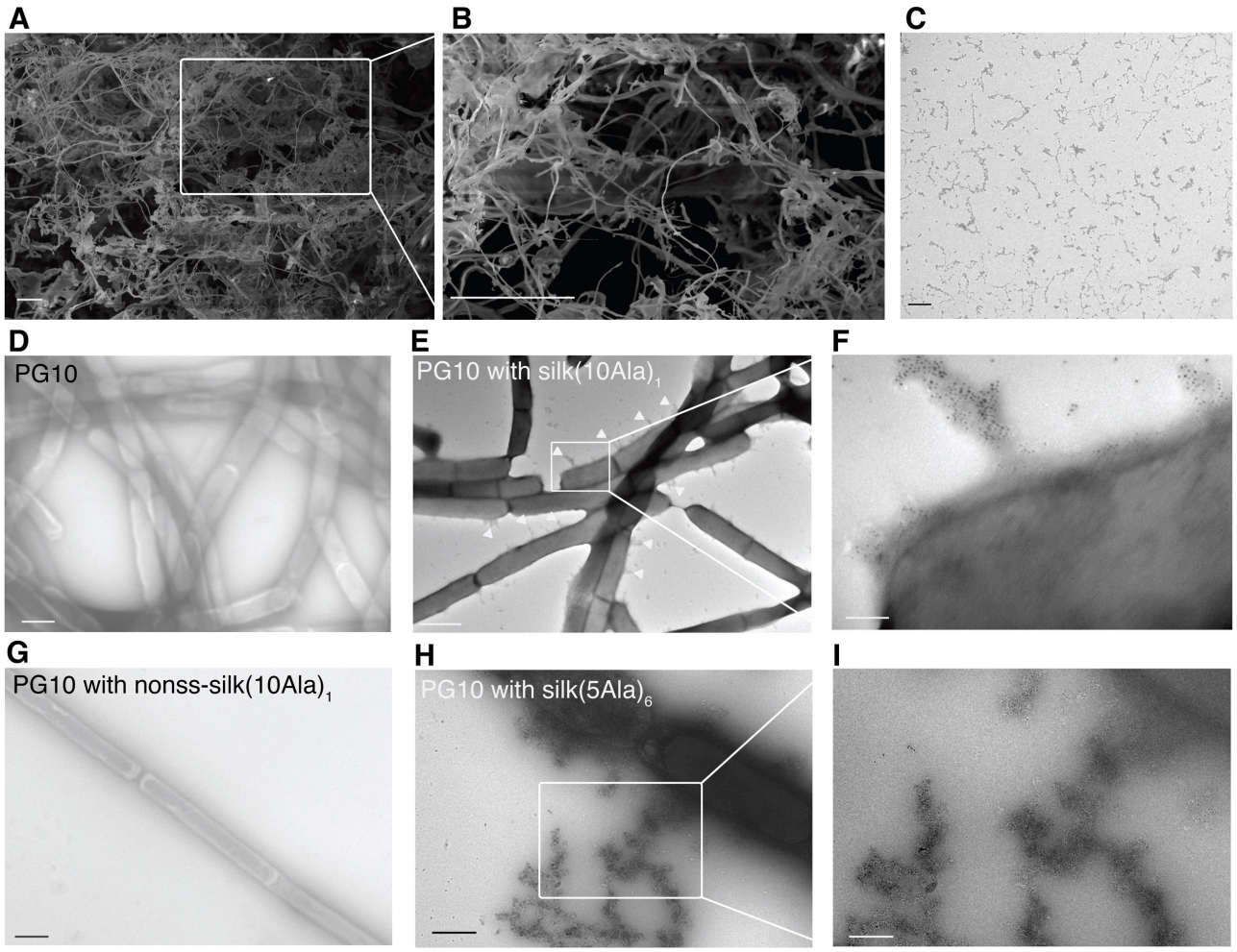

Figure 5. Electron microscopy. (A, B) Representative scanning electron micrographs of purified SCA-silk(10Ala)$_1$. White scale bar is 10 μm. Panel B is a zoom-in view of the white box in panel A. (C) Representative transmission electron micrograph of an identically prepared sample. Black scale bar is 1 μm. (D–I) Immunogold labeling of the silk(10Ala)$_1$ and silk(5Ala)$_6$ nanofibers on the *Bacillus* membrane surface. *B. subtilis* harbouring plasmids expressing different silk variants were induced, and cells were collected, fixed, stained with Ni-NTA-decorated gold nanoparticles, destained, and imaged. Images were obtained by transmission electron microscopy at distinct levels of magnification. High-contrast particles correspond to Ni-NTA-gold nanoparticles, which associate specifically with His-tagged proteins. Spike-like silk(10Ala)$_1$ fibers are indicated by white arrows on the panel E. Scale bars are 1 μm (D, E, G), 500 nm (H), 200 nm (I) and 100 nm (F). *B. subtilis* cells without plasmids (D) and with plasmids expressing non-secretory silk(10Ala)$_1$ (G) were used as negative controls.

Material properties of silk hydrogels

To isolate silk(10Ala)$_1$, we combined spent media (containing the secreted fraction) with Ni-NTA resin, performed affinity purification, and then dialyzed the eluted fractions into PBS buffer. This initially produced a modest yield (3.7 ± 1.7 mg/L). We later found that substantial losses were incurred during the affinity purification at high dilutions, and found that isolated yields could be substantially improved when spent media was first pre-concentrated prior to affinity purification (between 16–34 mg/L, Figure S8A). Like other self-assembling peptides, SCA-silk(10Ala)$_1$ is a porous solid (Figure S8B), that when suspended in water forms a viscous solution that remains aloft in its vial after the inversion test, but with a viscosity only slightly larger (1.5–10-fold) than water and with very small loss and storage moduli (Figure S9A–C).[49–51] However, upon concentrating the SCA-silk(10Ala)$_1$ solution in a centrifugal concentrator at 4 °C, we found that it spontaneously phase separated from the bulk aqueous phase, forming a dense yellow hydrogel at the bottom of the filter (Figure 7A).[52,53] We verified the amyloid morphology of the SCA-silk(10Ala)$_1$ hydrogel using Congo red staining, consistent with the previous reported feature of silk (Figure S10).[54,55] Rheological investigations of the isolated material confirmed that SCA-silk(10Ala)$_1$ forms a reversible hydrogel with dynamic crosslinks at lower temperatures ($\approx$4 °C, Figure 7B) with a shear strain curve prototypical of protein hydrogels (Figure 7C). Specifically, it exists as a gel at shear strains below 5 %, and can reversibly reform after the shear strain is stopped, exhibiting rheological self-healing (Figure S11A–B). Whilst the dynamic moduli of this hydrogel are not high-performance per se, they are comparable to silk hydrogels composed of peptides $\approx$16-fold longer (i.e., silk(8Ala)$_{16}$) processed with previously-

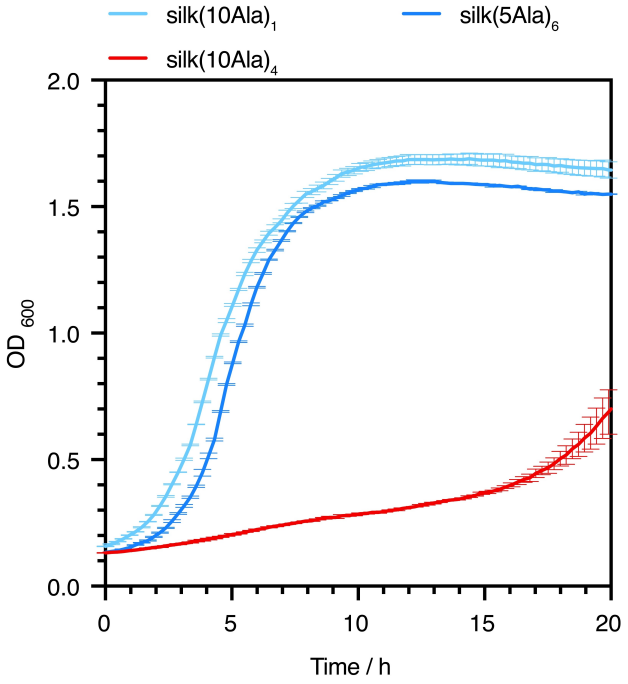

Figure 6. Growth Curve of *B. subtilis* PG10 secreting different variants of silk. Averaged time courses measuring optical density of bacterial culture in 2xYT media with 1 mM IPTG in a microplate reader equipped with shaking and incubation at 37 °C. Error bar represent std dev from biological replicates ($n = 3$).

reported methods;[38] this suggests that autonomous processing via SCA potentially provides a boost to mechanical properties.

Production of silk-based engineered living materials

A new paradigm in biomaterials is that of engineered living materials (ELMs), in which viable cells are additionally part of the material matrix in addition to secreted proteins or other biomacromolecules.[9,56,57] These types of biomaterials have a number of attractive properties, such as the ability to self-regenerate, respond to their environments, and perform biologically useful functions. Having observed that silk assemblies form directly on membranes (with that of silk$(5Ala)_6$ resulting in particularly intricate networks, cf. Figure 5H–I), we wondered if *Bacilli* expressing these proteins would be amenable to forming a living material. A culture of cells expressing and secreting silk$(5Ala)_6$ was filtered and partially dried onto a 0.22 μm filter, resulting in a mat that we collected and could process by extrusion (Figure 7D).[58,59] This material was 2-fold stiffer than the one formed by *Bacilli* that were not transformed (Figure 7E), and could also regenerate itself even after it was air dried for 6 d (Figure S14). Scanning electron micrographs of the ELM showed communities of cells connected by projections (Figure 7F), with denser networks forming with silk$(5Ala)_6$ than with silk$(10Ala)_1$, consistent with TEM images of individual cells performing SCA (cf. Figure 5). These experiments show that in addition to processing silk fibers for complete secretion (through signal peptidase activity), SCA also results in fibrous projections retained on the plasma membrane useful for modulating the material properties of *Bacilli* themselves.

Conclusion

Commercial investment in "brewed materials" and "engineered living materials" underscores the high current interest in engineered protein biomaterials.[1,4,60] Whilst the last decade has seen progress in expressing silk proteins,[10,11,29,38,61] modifying their sequences,[32,62,63] and developing biomimetic processing workflows,[31,47] the notion that microbes could autonomously synthesize, secrete, and process protein materials has not been widely discussed. Here we demonstrate the feasibility of this approach through secretion-catalyzed assembly (SCA) on *B. subtilis*. These studies show that SecYEG-mediated translocation in Gram positive bacteria (utilizing the TasAss and the SipW signal peptidase) is a promising exit route for fibrous proteins. We have reported decent protein yields from shaker-flask cultures with standard IPTG-induced expression (upto 34 mg/L; Figures S8A, S13), suggesting the system is primed for scale-up through a dedicated bioreactor optimization effort and gene circuit engineering. The secretion mechanism, which involves a membrane-bound intermediate via the TasA signal peptide, additionally promotes autonomous processing of silk peptides on the plasma membrane, which in turn can be controlled through linker flexibility and signal peptidase activity. It is possible that the endogenous TasA biofilm also takes advantage of this assembly mechanism,[45] and that the kinetics of secretion and cleavage of the TasA signal and SipW signal peptidase are well-tuned for this purpose. If so, these traits combined with their orthogonality to other signals/peptidases render them a promising tool for biomaterial secretion.

At present, the mechanical properties of silk$(10Ala)_1$ hydrogels and silk$(5Ala)_6$-*Bacillus* ELMs are not superlative, and it is likely the mechanical properties of these protein fibers would be enhanced if cells were engineered to secrete peptides at higher levels and with greater chain-lengths than silk$(10Ala)_1$ or silk$(5Ala)_6$. Highly repetitive gene sequences are known to be problematic in *Bacillus* because of its high recombinogenicity. To address this challenge, a key future direction of ours is to couple secretion-catalyzed assembly with loopable translation (in which repetitive proteins are synthesized by iterative ribosomal translation on circularized mRNA),[64] which we have recently shown works even more efficiently in *B. subtilis* than in *E. coli*.[65] In this regard, another critical feature of SecYEG translocation is its capacity to operate cotranslationally; hence, in this mode silk peptides of indefinite length (as produced by loopable translation) should still be secretable. Looking forward, we believe that autonomous biomaterial assembly will have numerous applications in self-healing materials, probiotic tissue regeneration, and sustainable biodegradable polymers.

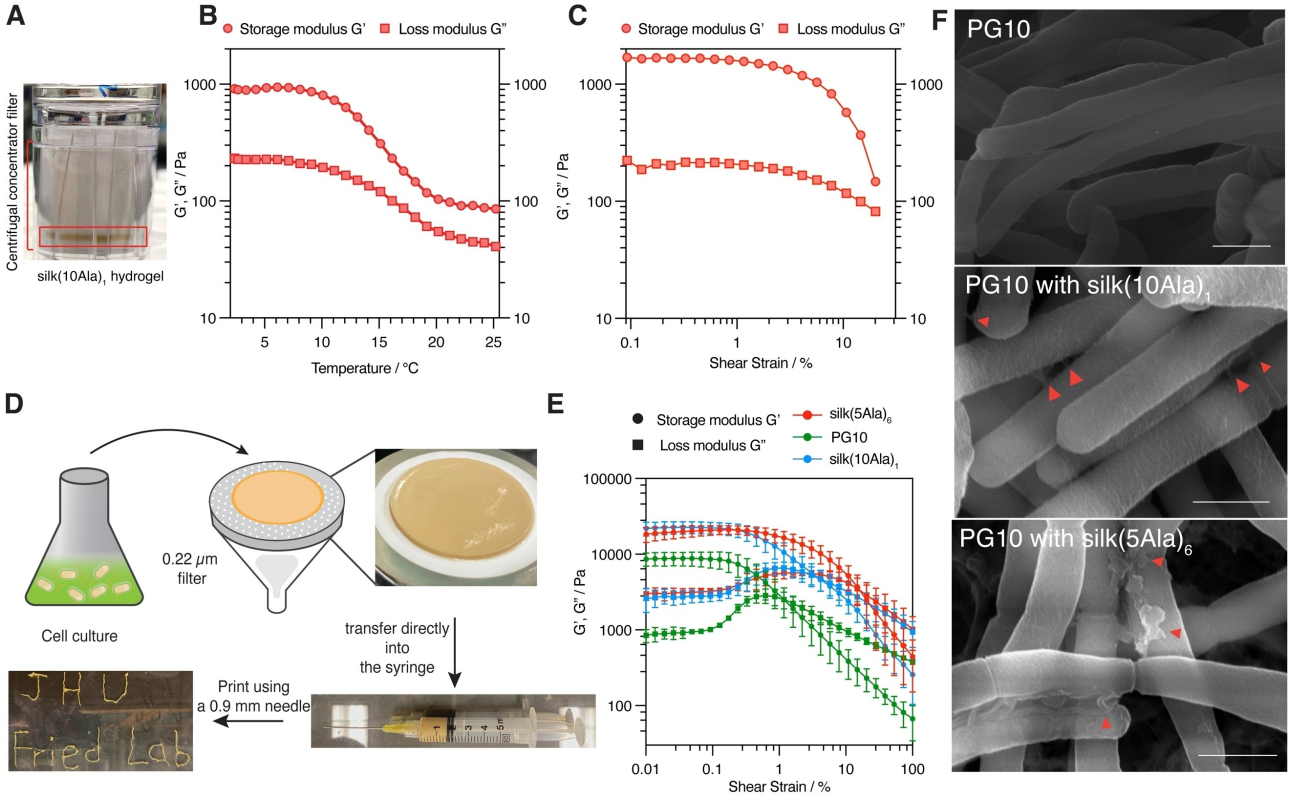

Figure 7. Characterization of SCA-silk hydrogels and ELMs. (A–C) Rheological properties of SCA-silk(10Ala)$_1$ hydrogel: (A) Representative image of SCA-silk(10Ala)$_1$ forming hydrogel after centrifugation at 4 °C; (B) Temperature sweep measurement of dynamic moduli of SCA-silk(10Ala)$_1$ hydrogel with angular frequency at 10 rad/s and shear strain at 1%; (C) Strain sweep measurement of SCA-silk(10Ala)$_1$ hydrogel with angular frequency at 10 rad/s, 4 °C. (D–F) Silk-scaffolded ELMs: (D) Illustration of the process for making silk-scaffold ELM. PG10 culture expressing silk overnight were subjected for filtration using a 0.22 μm pore size membrane. The collected material can be transferred directly into a 5 mL syringe equipped with a 0.9 mm needle. The material can be further extruded and printed into shapes. The images showed here are samples of silk(5Ala)$_6$. (E) Strain sweep measurement of silk-scaffold ELM with angular frequency at 10 rad/s. Error bar represent std dev from biological replicates ($n=3$). (F) Representative scanning electron micrographs of collected silk-scaffold ELM. Red arrows indicate where the silk fibers are. White scale bars are 1 μm.

Supporting Information

The authors have cited additional references within the Supporting Information.[66,67,76,77,68–75]

Acknowledgements

We would like to thank Robert Louder, Ya-Peng Yu, and the Johns Hopkins Integrated Imaging Center (IIC) for providing training and support with SEM and TEM. We also thank the Johns Hopkins Material Characterization and Processing facility (MCP) for support with rheology. We acknowledge Yihao Chen (JHU Physics and Astronomy) for advice on acquisition and interpretation of rheological measurements. We also want to thank Prof. Jörg Stülke (University of Göttingen, Germany), Prof. Sabine Schneider (Ludwig Maximilian University Munich) and Prof. David L. Kaplan (Tufts University) for their kind gifts of *B. subtilis* strains and plasmids. M. E. J. acknowledges support from the NIH (R35-GM133644). S. D. F. acknowledges support from the NIH Director's New Innovator Award (DP2-GM140926) and an NSF CAREER grant from the Division of Molecular and Cellular Biology (MCB2045844).

Conflict of Interest

The authors declare no conflict of interest.

Data Availability Statement

The data that support the findings of this study are available in the supplementary material of this article.

Keywords: Engineered Living Materials · Microbial Bioengineering · Protein Biomaterials · Secretion · Silk Fibers

[1] M. Jones, A. Mautner, S. Luenco, A. Bismarck, S. John, *Mater. Des.* **2020**, *187*, 108397.
[2] K. Numata, *Polym. J.* **2020**, *52*, 1043–1056.

[3] N. Kono, H. Nakamura, M. Mori, Y. Yoshida, R. Ohtoshi, A. D. Malay, D. A. Pedrazzoli Moran, M. Tomita, K. Numata, K. Arakawa, *Proc. Natl. Acad. Sci. USA* **2021**, *118*, e2107065118.

[4] D. Lips, *Emerg. Top. Life Sci.* **2021**, *5*, 711–715.

[5] T. Dvir, B. P. Timko, D. S. Kohane, R. Langer, *Nat. Nanotechnol.* **2011**, *6*, 13–22.

[6] D. R. Whittall, K. V. Baker, R. Breitling, E. Takano, *Trends Biotechnol.* **2021**, *39*, 560–573.

[7] C. H. Bowen, B. Dai, C. J. Sargent, W. Bai, P. Ladiwala, H. Feng, W. Huang, D. L. Kaplan, J. M. Galazka, F. Zhang, *Biomacromolecules* **2018**, *19*, 3853–3860.

[8] S. Molinari, R. F. Tesoriero, D. Li, S. Sridhar, R. Cai, J. Soman, K. R. Ryan, P. D. Ashby, C. M. Ajo-Franklin, *Nat. Commun.* **2022**, *13*, 5544.

[9] P. Q. Nguyen, N. M. D. Courchesne, A. Duraj-Thatte, P. Praveschotinunt, N. S. Joshi, *Adv. Mater.* **2018**, *30*, 1704847.

[10] D. M. Widmaier, D. Tullman-Ercek, E. A. Mirsky, R. Hill, S. Govindarajan, J. Minshull, C. A. Voigt, *Mol. Syst. Biol.* **2009**, *5*, 309.

[11] S. R. Fahnestock, L. A. Bedzyk, *Appl. Microbiol. Biotechnol.* **1997**, *47*, 33–39.

[12] S. R. Fahnestock, Z. Yao, L. A. Bedzyk, *Rev. Mol. Biotechnol.* **2000**, *74*, 105–119.

[13] A. Lazaris, S. Arcidiacono, Y. Huang, J. F. Zhou, F. Duguay, N. Chretien, E. A. Welsh, J. W. Soares, C. N. Karatzas, *Science* **2002**, *295*, 472–476.

[14] Q. Jin, F. Pan, C. F. Hu, S. Y. Lee, X. X. Xia, Z. G. Qian, *Metab. Eng.* **2022**, *70*, 102–114.

[15] X. X. Xia, Z. G. Qian, C. S. Ki, Y. H. Park, D. L. Kaplan, S. Y. Lee, *Proc. Natl. Acad. Sci. USA* **2010**, *107*, 14059–14063.

[16] J. M. V. D. H. Tjalsma, H. Antelmann, J. D. H. Jongbloed, P. G. Braun, E. Darmon, R. Dorenbos, J.-Y. F. Dubois, H. Westers, G. Zanen, W. J. Quax, O. P. Kuipers, S. Bron, M. Hecker, H. Tjalsma, H. Antelmann, J. D. H. Jongbloed, P. G. Braun, E. Darmon, R. Dorenbos, J.-Y. F. Dubois, H. Westers, G. Zanen, W. J. Quax, O. P. Kuipers, S. Bron, M. Hecker, J. M. Van Dijl, *Microbiol. Mol. Biol. Rev.* **2004**, *68*, 207–233.

[17] J. M. van Dijl, M. Hecker, *Microb. Cell Fact.* **2013**, *12*, 3.

[18] I. Hirose, K. Sano, I. Shioda, M. Kumano, K. Nakamura, K. Yamane, *Microbiology* **2000**, *146*, 65–75.

[19] J. D. H. Jongbloed, H. Antelmann, M. Hecker, R. Nijland, S. Bron, U. Airaksinen, F. Pries, W. J. Quax, J. M. Van Dijl, P. G. Braun, *J. Biol. Chem.* **2002**, *277*, 44068–44078.

[20] H. Antelmann, H. Tjalsma, B. Voigt, S. Ohlmeier, S. Bron, J. M. Van Dijl, M. Hecker, *Genome Res.* **2001**, *11*, 1484–1502.

[21] A. Diehl, Y. Roske, L. Ball, A. Chowdhury, M. Hiller, N. Molière, R. Kramer, D. Stöppler, C. L. Worth, B. Schlegel, M. Leidert, N. Cremer, N. Erdmann, D. Lopez, H. Stephanowitz, E. Krause, B. J. van Rossum, P. Schmieder, U. Heinemann, K. Turgay, Ü. Akbey, H. Oschkinat, *Proc. Natl. Acad. Sci. USA* **2018**, *115*, 3237–3242.

[22] J. Böhning, M. Ghrayeb, C. Pedebos, D. K. Abbas, S. Khalid, L. Chai, T. A. M. Bharat, *Nat. Commun.* **2022**, *13*, 7082.

[23] C. M. Scheidler, M. Vrabel, S. Schneider, *ACS Synth. Biol.* **2020**, *9*, 486–493.

[24] A. A. Toymentseva, K. Schrecke, M. R. Sharipova, T. Mascher, *Microb. Cell Fact.* **2012**, *11*, 143.

[25] T. T. P. Phan, H. D. Nguyen, W. Schumann, *J. Biotechnol.* **2013**, *168*, 32–39.

[26] T. P. J. Knowles, M. J. Buehler, *Nat. Nanotechnol.* **2011**, *6*, 469–479.

[27] F. Vollrath, D. P. Knight, *Nature* **2001**, *410*, 541–548.

[28] O. S. Tokareva, S. Lin, M. M. Jacobsen, W. Huang, D. Rizzo, D. Li, M. Simon, C. Staii, P. Cebe, J. Y. Wong, M. J. Buehler, D. L. Kaplan, *J. Struct. Biol.* **2014**, *186*, 412–419.

[29] J. T. Prince, K. P. McGrath, C. M. DiGirolamo, D. L. Kaplan, *Biochemistry* **1995**, *34*, 10879–10885.

[30] C. H. Bowen, T. J. Reed, C. J. Sargent, B. Mpamo, J. M. Galazka, F. Zhang, *ACS Synth. Biol.* **2019**, *8*, 2651–2658.

[31] M. Andersson, Q. Jia, A. Abella, X. Y. Lee, M. Landreh, P. Purhonen, H. Hebert, M. Tenje, C. V. Robinson, Q. Meng, G. R. Plaza, J. Johansson, A. Rising, *Nat. Chem. Biol.* **2017**, *13*, 262–264.

[32] S. Szela, P. Avtges, R. Valluzzi, S. Winkler, D. Wilson, D. Kirschner, D. L. Kaplan, *Biomacromolecules* **2000**, *1*, 534–542.

[33] A. Müller, M. Wenzel, H. Strahl, F. Grein, T. N. V. Saaki, B. Kohl, T. Siersma, J. E. Bandow, H. G. Sahl, T. Schneider, L. W. Hamoen, *Genome Res.* **2016**, 289–299.

[34] R. A. Suárez, J. Stülke, J. M. Van Dijl, *ACS Synth. Biol.* **2019**, *8*, 99–108.

[35] A. Y. Van Tilburg, A. J. Van Heel, J. Stülke, N. A. W. De Kok, A. S. Rueff, O. P. Kuipers, *ACS Synth. Biol.* **2020**, *9*, 1833–1842.

[36] T. Lefèvre, S. Boudreault, C. Cloutier, M. Pézolet, *Biomacromolecules* **2008**, *9*, 2399–2407.

[37] B. K. Bhunia, B. B. Mandal, *ACS Biomater. Sci. Eng.* **2019**, *5*, 870–886.

[38] V. J. Neubauer, V. T. Trossmann, S. Jacobi, A. Döbl, T. Scheibel, *Angew. Chem. Int. Ed.* **2021**, *60*, 11847–11851.

[39] D. Ebrahimi, O. Tokareva, N. G. Rim, J. Y. Wong, D. L. Kaplan, M. J. Buehler, *ACS Biomater. Sci. Eng.* **2015**, *1*, 864–876.

[40] M. Heim, D. Keerl, T. Scheibel, *Angew. Chem. Int. Ed.* **2009**, *48*, 3584–3596.

[41] O. S. Rabotyagova, P. Cebe, D. L. Kaplan, *Macromol. Biosci.* **2010**, *10*, 49–59.

[42] B. Mishra, M. E. Johnson, *J. Chem. Phys.* **2021**, *154*, 194101.

[43] H. T. McMahon, E. Boucrot, *Nat. Rev. Mol. Cell Biol.* **2011**, *12*, 517–533.

[44] J. Halatek, F. Brauns, E. Frey, *Philos. Trans. R. Soc. B Biol. Sci.* **2018**, *373*, 20170107.

[45] S. Lin, S. Ryu, O. Tokareva, G. Gronau, M. M. Jacobsen, W. Huang, D. J. Rizzo, D. Li, C. Staii, N. M. Pugno, J. Y. Wong, D. L. Kaplan, M. J. Buehler, *Nat. Commun.* **2015**, *6*, 6892.

[46] A. P. Kiseleva, P. V. Krivoshapkin, E. F. Krivoshapkina, *Front. Chem.* **2020**, *8*, 554.

[47] I. Greving, M. Cai, F. Vollrath, H. C. Schniepp, *Biomacromolecules* **2012**, *13*, 676–682.

[48] Q. Lu, H. Zhu, C. Zhang, F. Zhang, B. Zhang, D. L. Kaplan, *Biomacromolecules* **2012**, *13*, 826–832.

[49] A. N. Moore, J. D. Hartgerink, *Acc. Chem. Res.* **2017**, *50*, 714–722.

[50] S. Lee, T. H. T. Trinh, M. Yoo, J. Shin, H. Lee, J. Kim, E. Hwang, Y. B. Lim, C. Ryou, *Int. J. Mol. Sci.* **2019**, *20*, 5850.

[51] A. Levin, T. A. Hakala, L. Schnaider, G. J. L. Bernardes, E. Gazit, T. P. J. Knowles, *Nat. Chem. Rev.* **2020**, *4*, 615–634.

[52] X. Xu, H. Cölfen, *Nanomaterials* **2021**, *11*, 333.

[53] Y. Chen, S. A. Rogers, S. Narayanan, J. L. Harden, R. L. Leheny, *Phys. Rev. Mater.* **2020**, *4*, 035602.

[54] T. Arndt, G. Greco, B. Schmuck, J. Bunz, O. Shilkova, J. Francis, N. M. Pugno, K. Jaudzems, A. Barth, J. Johansson, A. Rising, *Adv. Funct. Mater.* **2022**, *32*, 2200986.

[55] A. Nova, S. Keten, N. M. Pugno, A. Redaelli, M. J. Buehler, *Nano Lett.* **2010**, *10*, 2626–2634.

[56] S. Molinari, R. F. Tesoriero, C. M. Ajo-Franklin, *Matter* **2021**, *4*, 3095–3120.

[57] R. J. Jones, E. A. Delesky, S. M. Cook, J. C. Cameron, M. H. Hubler, W. V. Srubar III in *Engineered Living Materials, Vol. 1* (Ed.: W. V. Srubar III), Springer, Berlin, **2022**, pp. 187–216.

[58] N. M. Dorval Courchesne, A. Duraj-Thatte, P. K. R. Tay, P. Q. Nguyen, N. S. Joshi, *ACS Biomater. Sci. Eng.* **2017**, *3*, 733–741.

[59] A. M. Duraj-Thatte, A. Manjula-Basavanna, J. Rutledge, J. Xia, S. Hassan, A. Sourlis, A. G. Rubio, A. Lesha, M. Zenkl, A. Kan, D. A. Weitz, Y. S. Zhang, N. S. Joshi, *Nat. Commun.* **2021**, *12*, 6600.
[60] A. P. Liu, E. A. Appel, P. D. Ashby, B. M. Baker, E. Franco, L. Gu, K. Haynes, N. S. Joshi, A. M. Kloxin, P. H. J. Kouwer, J. Mittal, L. Morsut, V. Noireaux, S. Parekh, R. Schulman, S. K. Y. Tang, *Nat. Mater.* **2022**, *21*, 390–397.
[61] A. Heidebrecht, L. Eisoldt, J. Diehl, A. Schmidt, M. Geffers, G. Lang, T. Scheibel, *Adv. Mater.* **2015**, *27*, 2189–2194.
[62] S. C. Huang, Z. G. Qian, A. H. Dan, X. Hu, M. L. Zhou, X. X. Xia, *ACS Biomater. Sci. Eng.* **2017**, *3*, 1576–1585.
[63] W. Hwang, B. H. Kim, R. Dandu, J. Cappello, H. Ghandehari, J. Seog, *Langmuir* **2009**, *25*, 12682–12686.
[64] S. O. Lee, Q. Xie, S. D. Fried, *ACS Cent. Sci.* **2021**, *7*, 1736–1750.
[65] S. O. Lee, S. D. Fried, *U. S. Pat. Pending*, Application No.63/374,949.
[66] D. Akopian, K. Dalal, K. Shen, F. Duong, S. O. Shan, *J. Cell Biol.* **2013**, *200*, 397–405.
[67] M. Kahm, G. Hasenbrink, H. Lichtenberg-Frate, J. Ludwig, M. Kschischo, *J. Stat. Software* **2010**, *33*, 1–21.
[68] J. Schindelin, I. Arganda-Carreras, E. Frise, V. Kaynig, M. Longair, T. Pietzsch, S. Preibisch, C. Rueden, S. Saalfeld, B. Schmid, J. Y. Tinevez, D. J. White, V. Hartenstein, K. Eliceiri, P. Tomancak, A. Cardona, *Nat. Methods* **2012**, *9*, 676–682.
[69] E. I. Yakupova, L. G. Bobyleva, I. M. Vikhlyantsev, A. G. Bobylev, *Biosci. Rep.* **2019**, *39*, BSR20181415.
[70] T. U. Consortium, *Nucleic Acids Res.* **2023**, *51*, D523–D531.
[71] F. Sievers, A. Wilm, D. Dineen, T. J. Gibson, K. Karplus, W. Li, R. Lopez, H. McWilliam, M. Remmert, J. Söding, J. D. Thompson, D. G. Higgins, *Mol. Syst. Biol.* **2011**, *7*, 539.
[72] A. M. Waterhouse, J. B. Procter, D. M. A. Martin, M. Clamp, G. J. Barton, *Bioinformatics* **2009**, *25*, 1189–1191.
[73] I. Letunic, P. Bork, *Nucleic Acids Res.* **2021**, *49*, W293–W296.
[74] M. J. Varga, Y. Fu, S. Loggia, O. N. Yogurtcu, M. E. Johnson, *Biophys. J.* **2020**, *118*, 3026–3040.
[75] Y. Fu, O. N. Yogurtcu, R. Kothari, G. Thorkelsdottir, A. J. Sodt, M. E. Johnson, *J. Chem. Phys.* **2019**, *151*, 124115.
[76] S. Möller, M. D. R. Croning, R. Apweiler, *Bioinformatics* **2001**, *17*, 646–653.
[77] O. Arantes, D. Lereclus, *Gene* **1991**, *108*, 115–119.

Manuscript received: April 12, 2023
Accepted manuscript online: July 20, 2023
Version of record online: July 20, 2023